IEEE Access
Multidisciplinary ⋮ Rapid Review ⋮ Open Access Journal

Received 3 April 2023, accepted 8 May 2023, date of publication 19 May 2023, date of current version 31 May 2023.

Digital Object Identifier 10.1109/ACCESS.2023.3278025

RESEARCH ARTICLE

Robust Online Magnet Demagnetization Diagnosis in Asymmetrical Six-Phase AC Permanent Magnet Motor Drives

YASSER GRITLI[1,2], (Member, IEEE), CLAUDIO ROSSI[1], (Member, IEEE), GABRIELE RIZZOLI[1], MICHELE MENGONI[1], (Member, IEEE), ANGELO TANI[1], AND DOMENICO CASADEI[1]

[1]Department of Electrical, Electronic and Information Engineering "Guglielmo Marconi," University of Bologna, 40136 Bologna, Italy
[2]Department of Electrical Engineering, National Engineering School of Tunis, University of Tunis El Manar, Tunis 1002, Tunisia

Corresponding author: Yasser Gritli (yasser.gritli@unibo.it)

ABSTRACT Rotor magnets are critical components, which in case of fault, directly affect the performance of drives based on permanent magnet synchronous motors. Thus, monitoring the rotor magnets status is essential to ensure both high level of efficiency and service continuity. The present study focuses on the investigation of a new full-time domain-based method for the diagnosis of incipient rotor magnet demagnetization in a vector-controlled asymmetrical six-phase surface-mounted ac permanent magnet synchronous motor. The proposed strategy evaluates the rotor magnet demagnetization using a fault index derived from the control signals synthetized in the 5^{th} subspace, and already available in the control system platform. The main advantages of the proposed new strategy are its simplicity of implementation, and effectiveness even under time-varying operating conditions as the employed control signals in specific subspaces have a dc behavior. Extensive numerical simulations and experimental tests, carried out at different speed and load levels, have shown the validity of the proposed method, leading to an effective diagnostic procedure for a vector-controlled asymmetrical six-phase surface-mounted ac PMSM.

INDEX TERMS Condition monitoring, demagnetization, fault diagnosis, fault detection, asymmetrical six-phase PMSM, variable-speed drives.

I. INTRODUCTION

Multiphase Permanent Magnet Synchronous Motors (m-phase PMSMs) have gained significant interest by the research community in the last decade, becoming a feasible solution for several industry applications requiring high availability and fault tolerance capabilities [1], [2].

Although their prominent fault-tolerant ability against stator failures, m-phase PMSMs are potentially subjected to rotor magnet demagnetization (RMD). The main causes of RMD are high currents, high temperature, or both. The RMD can be a reversible or irreversible phenomenon. For the operating points above the well-known knee area of demagnetization, the loss of magnetization is recoverable when the temperature is decreased, and the RMD is a reversible phenomenon. If the operating point is driven below the knee area, the loss of magnetization is not recoverable at the original temperature of the magnets, leading to an irreversible RMD [3], [4], [5].

For m-phase PMSMs, the risk of exceeding the Curie temperature is unintentionally imposed by core losses, eddy current losses, and ohmic losses. For this type of machines, the stator field is often kept in quadrature with the rotor field produced by the magnets, and the stator field reaches its maximum values near the magnet trailing edges [6], [7]. Moreover, even if the rotor magnets are well designed, the magnetomotive force (mmf), due to large stator currents, will inevitably lead to a serious Reverse Field Demagnetization (RFD) on the magnet trailing edges, particularly when the rotor magnets are overheated. Thus, if not diagnosed at an

The associate editor coordinating the review of this manuscript and approving it for publication was Xiaokang Yin.

early stage, the degree of RMD will increase, which can limit the operating performance of the permanent magnets, leading to a reduced efficiency of the drive system [3], [4], [7].

Various techniques have been developed for the diagnosis of RMD in 3-phase PMSMs [5], [8], [9]. Traditionally, off-line techniques are based on the direct inspection and/or the use of a gaussmeter, so an assessment of the surface mounted PM flux pattern state can be inspected for possible cracks and/or demagnetization [4], [8]. However, off-line techniques have the drawback of requiring disassembly of the rotor and decoupling of the load.

Direct measurement of the rotor magnet temperature is of great importance, but it is not a trivial task due to the rotor rotation, which requires cabling through slip rings and brushes when contact sensors are used [10]. The accuracy of the sensed temperatures remains the main disadvantage of such a solution. To counter these limitations, there have been attempts using model-based techniques for estimating the PM temperature. In [11], a 2-D analytical model is developed to estimate the PM temperature distribution in the radial-axial plane. An hybrid analytical-thermal model was developed in [12] for estimating the PM temperature distribution in PMSM. Although the ability of these approaches they suffer from high latency and dependency on several motor parameters.

An alternative to the model-based approach for detecting RMD is a signal-based approach. In this sense, mechanical signals, such as shaft trajectory [13], and vibration analysis [14] have been successfully investigated. Electrical signal-based techniques have been proposed as potential alternatives, where motor current signature analysis (MCSA) [15], [16], [17], and voltage signature analysis (VSA) [15], [18], [19] have shown very interesting results. Magnetic flux analysis, using fluxgate sensors, has been proposed in [20], where leakage flux analysis has revealed more accurate and reliable results than those of back-emf (BEMF) and current analysis for detecting RMD. Recently, Hall sensors have been proposed in [21] and [22] for effective detection of RMD. Although the immunity to noise and the advantageous low cost of implementation, fluxgate sensors and Hall sensors measurements are dependent on probe positions. More recently, a toroidal-yoke-type search coil was proposed in [23] for measuring the BEMF, where the RMD fault localization signals are computed by the output signals of three search coils.

Although the interesting results obtained by above techniques, the required invasive installation and/or the incurred cost limit their applicability.

In addition to the selection of the appropriate variables adopted to detect RMD, intensive research efforts have been focused on the use of signal processing techniques for characterizing RMD even in non-stationary conditions. Under steady-state conditions, reliable RMD fault indexes were established based on monitoring the spectral content of the signals derived from motor or associated converter variables [8], [24]. However, in time-varying conditions, the tracked frequency components are spread proportionally to the transient conditions. To cope with this issue, time–frequency analysis such as, Choi–Williams distribution analysis [16], Hilbert–Huang transform [17], or Continuous Wavelet Transform [25], have been recommended. However, latency and the amount of data required remains the main drawbacks of these techniques.

Although the important development in terms of stator fault detection and tolerance for m-phase PMSMs, RMD fault has not received up to now the attention that deserves. To the best knowledge of the authors, and according to the available literature, very few papers tried to investigate detection and/or fault-tolerant strategies devoted to m-phase PMSMs affected by RMD [26]. In [27], the flux-linkages of the stator phases are calculated using the field reconstruction method (FRM), and are analyzed by Fourier Transform for detecting RMD. Then, optimization tools are used for achieving the optimal currents which yield improving the output torque performance of the 5-phase PMSM under RMD. A novel integral terminal sliding mode flux-linkage observer is developed in [28] for detecting RMD for 5-phase PMSMs. In [29], the assessments of current and voltage signature analysis, for on-line monitoring of RMD in 5-phase PMSM drives, were established. It was shown that the amplitude variation of harmonic components present in both stator currents and voltages are sensitive diagnostic indexes for detecting RMD. Recently, analysis based on BEMF, zero sequence voltage component (ZSVC), and power factor have been identified in [30] as the most sensitive detection methods for 5-phase PM Assisted Synchronous Reluctance Machines affected by RMD.

For 6-PMSMs, RMD fault signature based on BEMF analysis has been proposed in [31]. More recently, a super-twisting algorithm-based sliding-mode Luenberger observer is proposed to reconstruct the RMD fault affecting a 6-PMSM in [32]. Following the approach adopted in [31], further investigations have been carried out in [33], revealing the high sensitivity of a fault index based on the contributions of the 5^{th} and 7^{th} harmonic tracked in the 5^{th} subspace as defined by Vector Space Decomposition (VSD) method used for the analysis of multiphase machines.

Even if signal-based strategies are the most adopted approaches, and despite of being prosperous in many aspects, most of the techniques listed above still have some drawbacks that are under investigations, namely, the dependency on dynamic operating conditions.

In this paper, a new rotor magnet demagnetization fault index for 6-phase PMSMs is proposed which provides the following advantages, namely:

1) capability of incipient rotor magnet demagnetization fault detection and quantification, even under time-varying conditions with a high sensitivity;
2) robustness against stator asymmetries and specifically high-resistance connections recognized as the main initiators of stator faults;

3) simplicity of implementation, since only variables already available in the control platform are used;
4) low memory requirement due to low sampling frequency required, which in turn reduces considerably the latency of time processing, leading to an effective on-line monitoring of the rotor magnet demagnetization fault evolution.

II. CONTROL SYSTEM OF THE SIX-PHASE PMSM

A. MACHINE MODEL

The machine investigated in this paper is a 30° asymmetrical six-phase surface-mounted ac PMSM, with two insulated three-phase windings. The developed model considers up to the eleventh spatial harmonic of the magnetic field in the air gap. Based on the concept of VSD and considering the adopted stator winding design with two isolated neutral points, the formulation of the stator voltage equations, in the stationary reference frame, can be limited to the 1st and 5th subspaces as [33]:

$$\bar{v}_{S1} = R_S \bar{i}_{S1} + \frac{d\bar{\phi}_{S1}}{dt}, \tag{1}$$

$$\bar{v}_{S5} = R_S \bar{i}_{S5} + \frac{d\bar{\phi}_{S5}}{dt}, \tag{2}$$

where $\bar{v}_{S\rho}$, $\bar{i}_{S\rho}$ and $\bar{\phi}_{S\rho}$ are the space vectors of the stator voltages, the stator currents and the flux-linkages, respectively, in the $\alpha_\rho-\beta_\rho$ plane ($\rho = 1$ and 5), whereas R_S is the resistance of the stator windings. The flux-linkage space vectors, expressed in the $\alpha_1-\beta_1$, and $\alpha_5-\beta_5$ planes, are given by

$$\begin{aligned}\bar{\phi}_{S1} &= L_{S1}\bar{i}_{S1} + \varphi_{M1}\left(e^{j(\gamma+\Delta\gamma)} + e^{-j\gamma}\right)e^{j\theta} \\ &+ \varphi_{M11}\left(e^{-j11(\gamma+\Delta\gamma)} + e^{j11\gamma}\right)e^{-j11\theta}, \end{aligned}\tag{3}$$

$$\begin{aligned}\bar{\phi}_{S5} &= L_{S5}\bar{i}_{S5} + \varphi_{M5}\left(e^{j5(\gamma+\Delta\gamma)} + e^{-j5\gamma}\right)e^{j5\theta} \\ &+ \varphi_{M7}\left(e^{-j7(\gamma+\Delta\gamma)} + e^{j7\gamma}\right)e^{-j7\theta}. \end{aligned}\tag{4}$$

In (3)-(4), the angle θ denotes the relative position between stator and rotor in electrical radians, $\Delta\gamma$ the demagnetized portion of the rotor magnets (Fig. 1), whereas L_{S1}, and L_{S5} are the α_1-β_1, and α_5-β_5 synchronous inductances, and the quantities φ_{Mh} ($h = 1, 5, 7, 11$) are given by

$$\varphi_{Mh} = \frac{2\mu_0 N_S L \tau H_M K_{WSh}}{h^2\pi^2}, \tag{5}$$

where N_S is the number of winding series-connected conductors, L is the stator and rotor core axial length, τ is the pole pitch, H_M is the magnitude of PM magnetic field square waveform, K_{WSh} is the winding coefficient, and h is the harmonic order.

By substituting (3) and (4) in (1) and (2), respectively, the voltage space vectors expressed in the $\alpha_1-\beta_1$ and $\alpha_5-\beta_5$ planes, can be written as:

$$\bar{v}_{S1} = R_S \bar{i}_{S1} + L_{S1}\frac{d\bar{i}_{S1}}{dt}$$

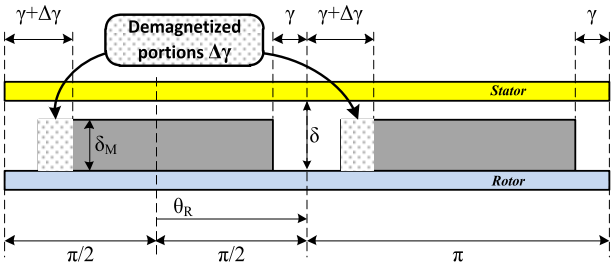

FIGURE 1. Illustration of a pair of surface-mounted permanent magnets under healthy ($\Delta\gamma = 0$), and demagnetized ($\Delta\gamma \neq 0$) conditions.

$$\begin{aligned} &+ \varphi_{M1}\left(e^{j(\gamma+\Delta\gamma)} + e^{-j\gamma}\right)j\omega e^{j\theta} \\ &- \varphi_{M11}\left(e^{-j11(\gamma+\Delta\gamma)} + e^{j11\gamma}\right)j11\omega e^{-j11\theta}, \end{aligned}\tag{6}$$

$$\begin{aligned}\bar{v}_{S5} &= R_S\bar{i}_{S5} + L_{S5}\frac{d\bar{i}_{S5}}{dt} \\ &+ \varphi_{M5}\left(e^{j5(\gamma+\Delta\gamma)} + e^{-j5\gamma}\right)j5\omega e^{j5\theta} \\ &- \varphi_{M7}\left(e^{-j7(\gamma+\Delta\gamma)} + e^{j7\gamma}\right)j\,7\omega e^{-j7\theta}, \end{aligned}\tag{7}$$

where ω is the mechanical speed in electrical rad/s.

As can be seen in (6), in the $\alpha_1-\beta_1$ plane two BEMFs harmonic components with angular speed $+\omega$ and -11ω are present, whereas in the $\alpha_5-\beta_5$ plane two BEMFs harmonic components with angular speed $+5\omega$ and -7ω can be found as shown in (7).

The electromagnetic torque T_{em} assumes the following expression, where four torque contributions are identified by their related spatial harmonics in the air gap [34]:

$$\begin{aligned}T_{em} &= 3\,p\varphi_{M1}\left[\bar{i}_{S1}\cdot j\left(e^{j(\gamma+\Delta\gamma)} + e^{-j\gamma}\right)\right]e^{j\theta} \\ &+ 15\,p\varphi_{M5}\left[\bar{i}_{S5}\cdot j\left(e^{j5(\gamma+\Delta\gamma)} + e^{-j5\gamma}\right)\right]e^{j5\theta} \\ &+ 21\,p\varphi_{M7}\left[\bar{i}^*_{S5}\cdot j\left(e^{j7(\gamma+\Delta\gamma)} + e^{-j7\gamma}\right)\right]e^{j7\theta} \\ &+ 33\,p\varphi_{M11}\left[\bar{i}^*_{S1}\cdot j\left(e^{j11(\gamma+\Delta\gamma)} + e^{-j11\gamma}\right)\right]e^{j11\theta}, \end{aligned}\tag{8}$$

where p is the number of pole pairs and $(\cdot)$ denotes the scalar product.

B. CONTROL SCHEME

The proposed control scheme is an improved FOC (IFOC), which is based on multiple synchronous proportional-integral (PI) regulators, allowing a speed control of the 6-phase PMSM, and providing RMD diagnosis (Fig. 2).

In the block diagram of Fig. 2, the reference current $i_{S1d,ref}$ is usually set to zero according to a maximum torque per Ampere strategy, and the reference current $i_{S1q,ref}$ is obtained by the regulator $\mathrm{PI_o}$ of the speed loop. The reference signals $i_{S5d,ref}$, $i_{S5q,ref}$ are kept equal to zero to eliminate the second and third disturbing terms in torque equation (8).

To design a specific current controller able to ensure a precise tracking of the reference currents, it is useful to

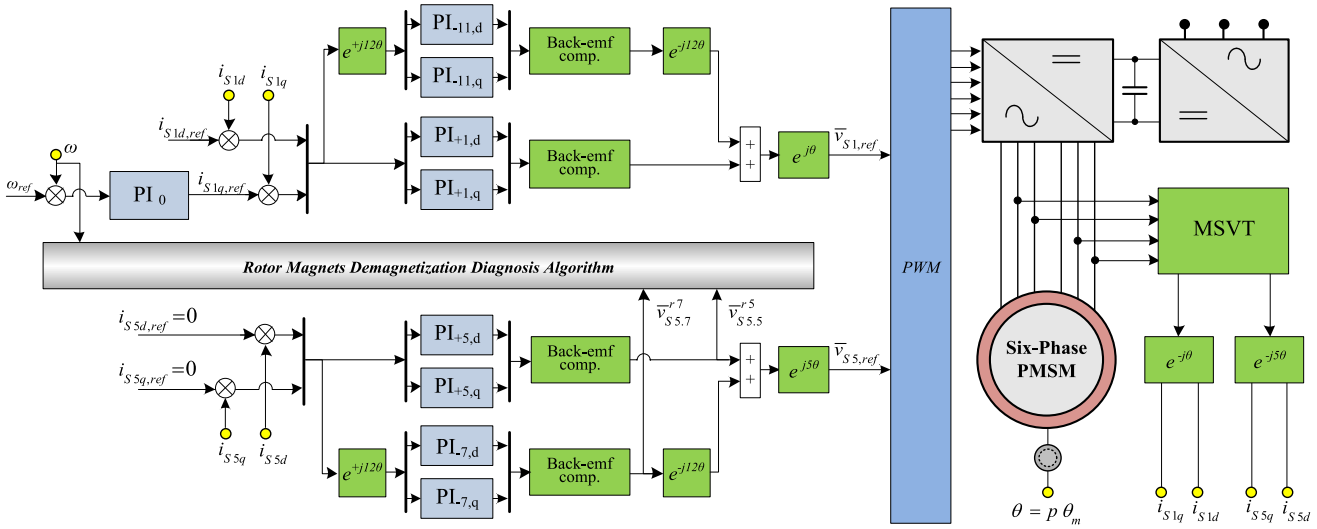

FIGURE 2. Block diagram of the IFOC scheme.

reformulate the stator voltage equations (6) and (7) in two different rotating reference frames d_1-q_1 and d_5-q_5, respectively, as follows:

$$\begin{aligned}\bar{v}_{S1}^{r1} &= R_S \bar{i}_{S1}^{r1} + L_{S1}\frac{d\bar{i}_{S1}^{r1}}{dt} + j\omega L_{S1}\bar{i}_{S1}^{r1} \\ &+ \varphi_{M1}\left(e^{j(\gamma+\Delta\gamma)} + e^{-j\gamma}\right)j\omega \\ &- \varphi_{M11}\left(e^{-j11(\gamma+\Delta\gamma)} + e^{j11\gamma}\right)j11\omega e^{-j12\theta}, \qquad (9)\\ \bar{v}_{S5}^{r5} &= R_S \bar{i}_{S5}^{r5} + L_{S5}\frac{d\bar{i}_{S5}^{r5}}{dt} + j\omega L_{S5}\bar{i}_{S5}^{r5} \\ &+ \varphi_{M5}\left(e^{j5(\gamma+\Delta\gamma)} + e^{-j5\gamma}\right)j5\omega \\ &- \varphi_{M7}\left(e^{-j7(\gamma+\Delta\gamma)} + e^{j7\gamma}\right)j\,7\omega e^{-j12\theta}. \qquad (10)\end{aligned}$$

The d_1-q_1 reference frame rotates with angular speed ω and the position of the d_1 axis is θ, whereas the d_5-q_5 reference frame rotates with angular speed 5ω and the position of the d_5 axis is 5θ. The subscript ("$S1$" and "$S5$") identifies the subspace, whereas the superscripts "$r1$" and "$r5$" are used to specify the rotating reference frame in which the space vectors are represented (d_1-q_1 and d_5-q_5, respectively). Note that, in the following, an additional rotating reference frame (d_7-q_7), synchronous with the 7th harmonic of the BEMF in subspace 5, and identified with the superscript "$r7$," will be adopted.

In (9) and (10) the effect of the BEMF harmonic components on the stator currents in healthy conditions ($\Delta\gamma = 0$) and under RMD ($\Delta\gamma \neq 0$) is clearly emphasized.

As can be seen, a pair of BEMF harmonic components is present in each subspace (dc and -12ω in plane d_1-q_1, dc and -12ω in plane d_5-q_5). Consequently, since a PI regulator can ensure a tracking with zero error only with dc signals, eight proportional–integral (PI) regulators were implemented in four different rotating d-q reference frames. The PI regulators $PI_{+1,d}$ and $PI_{+1,q}$ are implemented in the d_1-q_1 rotor reference frame rotating at an angular speed of ω, whereas $PI_{-11,d}$ and $PI_{-11,q}$ are implemented in a reference frame rotating at an angular speed of -11ω. Similarly, $PI_{+5,d}$ and $PI_{+5,q}$ are implemented in the d_5-q_5 rotor reference frame rotating at $+5\omega$, whereas $PI_{-7,d}$, $PI_{-7,q}$ are implemented in a reference frame rotating at -7ω.

Note that no specific filter is required in the control scheme. In addition to the small implicit filtering effect due to the sampling of the digital control system, an intrinsic filtering action is related to the behavior of the PI regulators. However, this action does not affect phase and amplitude of the estimated BEMF since they are evaluated in synchronous reference frames as dc quantities.

The reference voltage space vectors $\bar{v}_{S1,ref}$ and $\bar{v}_{S5,ref}$ entering the PWM block are obtained exploiting the outputs of the current regulators and proper coordinate transformations.

The gate signals for the six inverter legs are determined by the PWM block using a double three-phase space vector PWM technique.

III. DC SPACE VECTOR BASED INDEX FOR DIAGNOSIS OF ROTOR MAGNET DEMAGNETIZATION

As emphasized by (3) and (4), demagnetized portion $\Delta\gamma$ of the magnets affects both phase and amplitude of the flux-linkage harmonic content and, in turn, also the stator voltages expressed in (6) and (7). In [33], the spectral analysis of the reference stator voltage space vectors, evaluated in the α_5–β_5 plane, has been proposed for processing a demagnetization fault index based on the amplitude contributions of the 5th and 7th voltage harmonics. Then, this fault index has proven to be effective in steady state conditions, showing some limitations in case of transient conditions. In fact,

examining $\bar{v}_{S5}$ expressed by (7), it is evident that the impact of the 5th and 7th harmonic, under RMD, is speed-dependent which may affect the accuracy of the expected RMD fault index for different constant speed operating points. The situation becomes much more complicated under speed-transient conditions, leading to a spreading in magnitude and frequency of the above fault components of interest, and making their detection through a frequency domain analysis impossible. To cope with the above limitations, a new RMD diagnostic index based on (10) is defined in this section.

Under the assumption of the current space vector $\bar{i}_{S5}$ kept equal to zero for reducing the torque ripple in the proposed IFOC, (10) becomes

$$\bar{v}_{S5}^{r5} = \bar{e}_{5.5} + \bar{e}_{5.7} e^{-j12\theta}, \tag{11}$$

where $\bar{e}_{5.5}$ and $\bar{e}_{5.7}$, representative of the 5th and 7th BEMF harmonic components, respectively, are expressed by

$$\bar{e}_{5.5} = j5\omega\varphi_{M5}\left(e^{j5(\gamma+\Delta\gamma)} + e^{-j5\gamma}\right), \tag{12}$$

$$\bar{e}_{5.7} = -j7\omega\varphi_{M7}\left(e^{-j7(\gamma+\Delta\gamma)} + e^{j7\gamma}\right). \tag{13}$$

The current $\bar{i}_{S5}$, as well as its error, are affected by the 5th BEMF harmonic component, but this current error in a reference frame rotating at 5ω will become a dc quantity, so the regulators $\text{PI}_{+5\text{d}}$ and $\text{PI}_{+5\text{q}}$ will generate a dc voltage named $\bar{v}_{S5.5}^{r5}$ in Fig. 2. If the current regulators $\text{PI}_{+5\text{d}}$ and $\text{PI}_{+5\text{q}}$, work properly for zeroing the current error, $\bar{v}_{S5.5}^{r5}$ will approach the value of $\bar{e}_{5.5}$ given in (12). The current error of $\bar{i}_{S5}$ is also affected by the 7th BEMF harmonic component, which in d_5-q_5 generates a disturbance at -12ω. This disturbance cannot be properly compensated by regulators $\text{PI}_{+5\text{d}}$ and $\text{PI}_{+5\text{q}}$. To this aim, the current error in Fig. 2 is also multiplied by $e^{+j12\theta}$, so the disturbance due to the 7th BEMF harmonic will become a dc quantity, which through regulators $\text{PI}_{-7\text{d}}$ and $\text{PI}_{-7\text{q}}$ will generate a dc voltage named $\bar{v}_{S5.7}^{r7}$ in Fig. 2. If the current regulators $\text{PI}_{-7\text{d}}$ and $\text{PI}_{-7\text{q}}$, work properly for zeroing the current error, $\bar{v}_{S5.7}^{r7}$ will approach the value of $\bar{e}_{5.7}$ given in (13).

To take advantage of both amplitude and phase variations of the dc space vectors $\bar{v}_{S5.5}^{r5}$ and $\bar{v}_{S5.7}^{r7}$, due to the effect of demagnetized portion $\Delta\gamma$, an appropriate diagnostic dc space vector-based index F_{dem} is here proposed as

$$F_{dem} = F_5 + F_7, \tag{14}$$

in which F_5 and F_7 are the contributions representative of the 5th and 7th harmonics, respectively, formulated as

$$F_5 = \left\| \Delta\bar{v}_{S5.5}^{r5} \right\| \left| \omega^{-1} \right|, \tag{15}$$

$$F_7 = \left\| \Delta\bar{v}_{S5.7}^{r7} \right\| \left| \omega^{-1} \right|, \tag{16}$$

where the BEMF dc diagnosis space vectors $\Delta\bar{v}_{S5.5}^{r5}$ and $\Delta\bar{v}_{S5.7}^{r7}$ are computed as in the following (see Fig. 3):

$$\Delta\bar{v}_{S5.5}^{r5} = \bar{v}_{S5.5}^{r5} - \bar{v}_{S5.5_0}^{r5}, \tag{17}$$

$$\Delta\bar{v}_{S5.7}^{r7} = \bar{v}_{S5.7}^{r7} - \bar{v}_{S5.7_0}^{r7}. \tag{18}$$

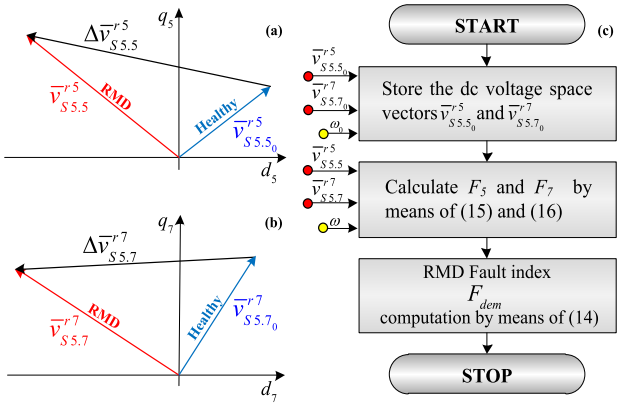

FIGURE 3. Illustration of the BEMF diagnostic space vectors (a) $\Delta\bar{v}_{S5.5}^{r5}$ and (b) $\Delta\bar{v}_{S5.7}^{r7}$ in the $d_5 - q_5$ and $d_7 - q_7$ planes, respectively. (c) Flowchart showing the implementation of the proposed RMD fault index.

Note that the subscript "0" identifies the values of the dc BEMF space vectors in healthy conditions.

Finally, after further developments of (15) - (18), using the expressions (12) and (13) under healthy and faulty conditions, the RMD fault index F_{dem} given in (14) becomes

$$F_{dem} = 5\sqrt{2}\varphi_{M5}\sqrt{1 - cos\,(5\Delta\gamma)} + 7\sqrt{2}\varphi_{M7}\sqrt{1 - cos\,(7\Delta\gamma)} \tag{19}$$

Based on (19), it is very useful to underline that under healthy rotor magnets ($\Delta\gamma = 0$), the RMD fault index F_{dem} becomes equal to zero, leading to a clear characterization of the healthy case. Whereas, under RMD ($\Delta\gamma \neq 0$), the RMD fault index F_{dem} will become different from zero, leading to a clear detection and quantification of the fault extent for small demagnetization angles.

It is important to note at this stage that the sensitivity of the proposed fault index is not only maximized by summing the amplitude variations of the dc voltage space vectors $\bar{v}_{S5.5}^{r5}$ and $\bar{v}_{S5.7}^{r7}$ representative of the 5th and 7th harmonic contributions, but also by their phase variations, respectively. Moreover, considering the speed normalization adopted in (15) and (16), the proposed RMD fault index becomes independent of the speed level.

Fig. 4-a shows the spectra of the space vector $\bar{v}_{S5,ref}$, under two different constant speed levels. Observing the amplitude variations of the 7th and 5th harmonics, corresponding to the two speed levels, respectively, the speed-dependency of the two harmonics is clearly evidenced. However, for the same operating conditions adopted in Fig. 4-a, the proposed speed normalized dc space vectors $\bar{v}_{S5.5}^{r5}$, (Fig. 4-b) and $\bar{v}_{S5.7}^{r7}$ (Fig. 4-c), show constant values for the two different speed levels, leading to a clear immunity against the speed operating condition of the machine.

For the same operating conditions, and 10% of rotor magnet demagnetization, the same quantities are reported in Figs. 4-d to 4-f, respectively, where the same conclusions

under healthy conditions are confirmed for the faulty case. Thus, the amplitude increments of the proposed speed normalized dc space vectors $\bar{v}^{r5}_{S5.5}$, and $\bar{v}^{r7}_{S5.7}$, from healthy (Figs. 4-b and 4-c) to faulty condition (Fig. 4-e and 4-f), confirm the sensitivity of the two quantities to RMD independently of the machine speed level.

In order to evaluate the combined amplitude and frequency speed-dependency of the space vector $\bar{v}_{S5,ref}$, and the dc space vectors $\bar{v}^{r5}_{S5.5}/\omega$ and $\bar{v}^{r7}_{S5.7}/\omega$, further numerical simulations under speed transient conditions were carried out with a speed variation ranging from 100 to 250 r/min. The corresponding spectra, under healthy and 10% of rotor magnet demagnetization, are depicted in Fig. 4-g to 4-i, respectively. As anticipated, the 7th and 5th harmonics are clearly affected by the well-known spreading effect in magnitude and frequency, making their detection through a spectral analysis of $\bar{v}_{S5,ref}$ impossible (Fig. 4-g). However, the same amplitude variation, of the dc space vector $\bar{v}^{r5}_{S5.5}$ at constant speed, from healthy (Fig. 4-b) to faulty (Fig. 4-e) conditions, is equal to the variation observed under transient condition (Fig. 4-h) from healthy to 10% of RMD. This result in transient condition is also confirmed for the dc space vector $\bar{v}^{r5}_{S5.7}$ (Fig. 4-i), when compared to the results obtained in steady-state conditions (Fig. 4-c and 4-f).

Finally, the obtained results under steady-state and transient conditions confirm the robustness of the speed normalized dc space vectors $\bar{v}^{r5}_{S5.5}$, and $\bar{v}^{r7}_{S5.7}$, and the sensitivity of the proposed fault index F_{dem} to RMD independently of the speed operating conditions.

Several simulations under different temperature conditions were made under healthy and different RMD levels of demagnetization. The simulations carried out were based on the principle of magnet remanence dependency on temperature expressed as follows:

$$B_R\left(T_0+\Delta T\right)=B_R\left(T_0\right)\left(1+\alpha_B\Delta T\right) \tag{20}$$

where T_0 is the basic temperature in rated condition, ΔT is the temperature rise with respect to the basic one, and α_B is the temperature coefficient of the permanent magnet material. For NdFeB magnets (the ones of our six-phase PM motor) $\alpha_B=-0.0012$.

Looking at Fig. 5, one can realize that in healthy conditions a temperature rise with respect to rated temperature, ranging from 0°C to 80°C, leads to a very negligible variation (∼0.0013 Wb) of the proposed RMD fault index F_{dem}, leading to a clear diagnosis of the healthy case.

Considering the same temperature rise under a large RMD of 14% ($\Delta\gamma=18.912°$), a variation of ∼0.0054 Wb occurs which does not affect the detection effectiveness of the proposed RMD fault index F_{dem}.

Finally, given that the required signals ($\bar{v}^{r5}_{S5.5}$ and $\bar{v}^{r7}_{S5.7}$), for calculating the proposed RMD fault index, are dc quantities, as a matter of fact, the proposed strategy is a full-time domain-based method, which does not require a time-consuming spectral analysis.

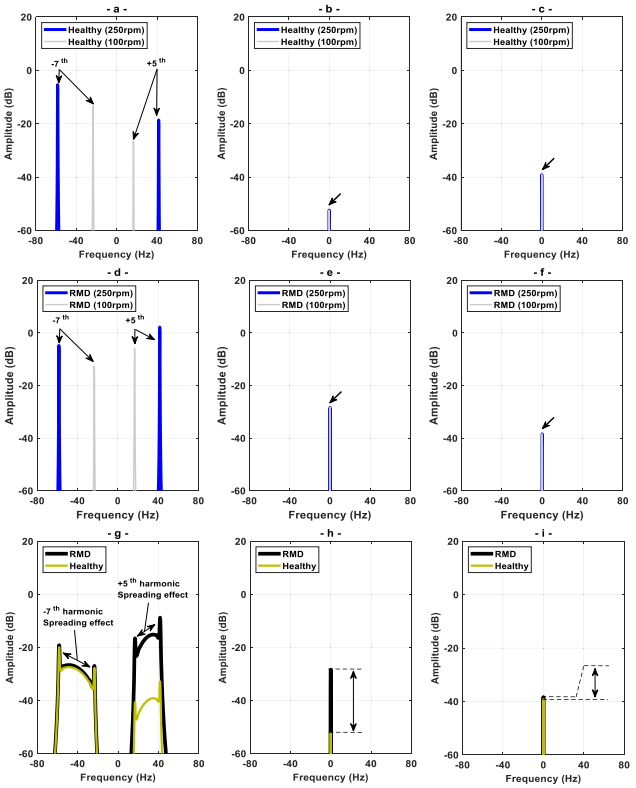

FIGURE 4. Spectral behaviors. From left to right, the space vector $\bar{v}_{S5,ref}$, and the dc space vectors $\bar{v}^{r5}_{S5.5}/\omega$ and $\bar{v}^{r7}_{S5.7}/\omega$. (a)-(c) Healthy motor for two different constant speed levels. (d-f) Motor with 10% of RMD for two different constant speed levels. (g-i) Healthy motor and 10% of RMD under a speed transient from 100 to 250 rpm.

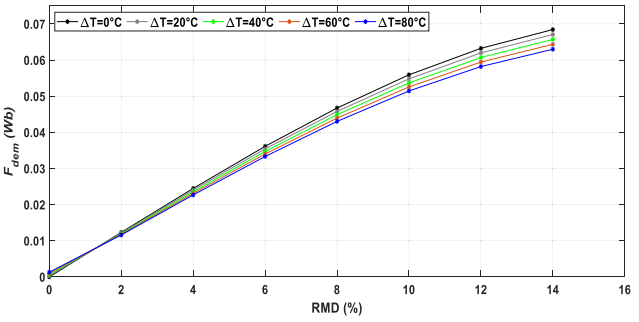

FIGURE 5. Simulation results: Temperature effect on the behavior of the proposed fault index F_{dem} under different RMD levels.

This is a significant improvement in terms of time-processing against a previous frequency-based technique [33] requiring spectral analysis.

Specifically, the two dc space vectors $\bar{v}^{r5}_{S5.5}$ and $\bar{v}^{r7}_{S5.7}$ are directly available on-line at the output of the current regulators (Fig. 2), whereas the second two dc space vectors $\bar{v}^{r5}_{S5.5_0}$ and $\bar{v}^{r7}_{S5.7_0}$ represents the same quantities evaluated in healthy condition (subscript "0") which allows an easy implementation of the BEMF diagnosis space vectors $\Delta\bar{v}^{r5}_{S5.5}$ and $\Delta\bar{v}^{r7}_{S5.7}$, expressed in (17) and (18), respectively. After applying the speed normalizations given by (15) and (16), the

TABLE 1. Six-phase PMSM parameters.

Parameter		
Rated torque	20	Nm
Phase resistance	0.36	Ohms
Rated current	10	A
Rated speed	1000	rpm
Pole number	4	-
Phase inductance	1.44	mH
Stator inner radius	150	mm
Stator outer radius	240	mm
Slot number	48	-
Stator winding pitch	165°	el. degrees
Magnet pole–arc	151°	el. degrees
Magnet radial thickness	5	mm

RMD fault index is easily computed on-line. Fig. 3-c illustrates the implementation flowchart for the proposed RMD fault index.

Note that, since this method is based on the evaluation of the BEMFs induced in the stator windings by the rotor magnets, it can be adopted, with a few adjustments, for the diagnosis of incipient rotor magnet demagnetization also for symmetrical six-phase PMSMs and six-phase IPM motors.

IV. SIMULATION AND EXPERIMENTAL RESULTS

Simulation and experimental results are provided in this section to verify the established analytical predictions of the proposed RMD fault index F_{dem}. Based on the VSD modeling principle of the six-phase PMSM described in the previous section, and the associated IFOC system (Fig. 2), a simulation scheme has been implemented in Matlab/Simulink® environment.

The implemented system allows a detailed investigation of the behavior of the controlled six-phase surface-mounted ac PMSM under healthy and faulty conditions. Specifically, the simulations have been carried out with healthy rotor magnets ($\Delta\gamma = 0°$) and, then, under partial RMD of $\Delta\gamma$, involving uniformly all the rotor magnets. The RMD was emulated by reducing the pole arc of all the rotor magnets by $\Delta\gamma$.

The parameters of the healthy motor, considered as reference, are listed in Table 1. They correspond to the parameters of the real healthy motor used for experiments.

The experimental test bench (Fig. 6) consists of a custom-designed six-phase MOSFET voltage source inverter (Fig. 6-b) feeding a six-phase PMSM. The MOSFETs are rated 300A and 100 V, and the dc bus voltage is of about 50 V. Two prototypes of asymmetrical six-phase surface mounted ac PMSM, with rotor magnets (Fig. 6-c) having different pole arc, were built. The two motors have been manufactured by a local company specialized in the construction of electrical machines, where the demagnetization fault was set on one motor by reducing the magnet pole–arc by 10°, corresponding to 6.62% of the healthy case. Design details of the healthy motor, considered as reference, are provided in [35].

The test motor is coupled to a three-phase induction motor acting as load. The proposed IFOC algorithm was implemented in a TMS–320F2812-based electronic control board (Fig. 6-d). The accuracy of the current sensors is of ±1.5%,

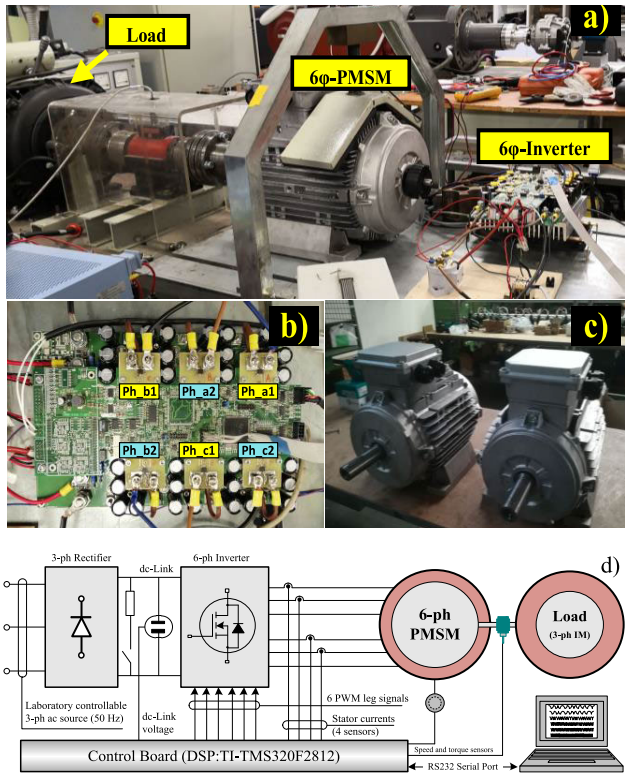

FIGURE 6. (a) Experimental test bench view; (b) Six-phase inverter. (c) Two prototypes. (d) Schematic diagram of the test bench.

with a linearity of ±1.5%, and a frequency bandwidth of (−3 dB) 80 kHz. The encoder resolution is of 2048 pulses per revolution.

The VSI switching frequency is of 5.5 kHz with a deadtime of 3.2 μs, whereas a sampling rate of 2.0 kHz for data acquisition was adopted. It should be noted that the effects of inverter dead times could represent a source of error in the proposed rotor magnet demagnetization algorithm, especially in the low-speed range. Therefore, a conventional dead time compensation algorithm is implemented in the control scheme.

As a preliminary investigation, the analysis was carried out by comparing the magnitude behavior of the dc voltage space vectors $\bar{v}^{r5}_{S5.5}/\omega$ and $\bar{v}^{r7}_{S5.7}/\omega$, under healthy rotor magnets ($\Delta\gamma = 0$), then, with magnets having a reduced pole arc ($\Delta\gamma = 10°$).

Simulation results are shown in Fig. 7, whereas the corresponding experimental results are reported in Fig. 8, where the motor was operating at 250 rpm and delivering the rated torque for all tests. For a sake of clear comparison, only the waveforms of the first phase currents a1 and a2 of each three-phase winding are reported.

Comparing the waveforms obtained under healthy (Fig. 7-a) and faulty (Fig. 7-d) conditions, it turns out that the stator phase currents are perfectly sinusoidal even under a 10° (6.62%) of RMD, confirming a good performance of the proposed IFOC scheme.

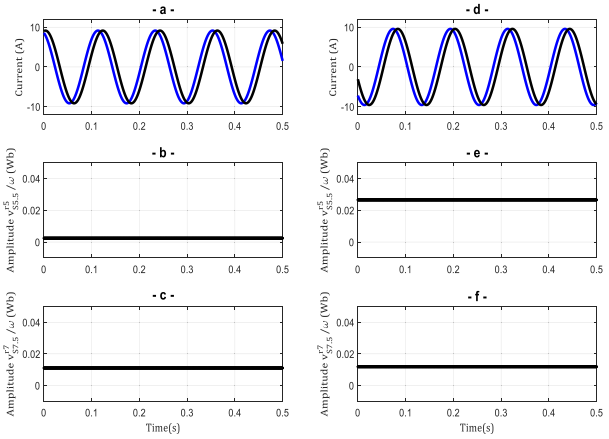

FIGURE 7. Simulation results: from top to bottom, waveforms of the stator currents in phase a1 and a2, magnitudes of the dc voltage space vectors $\bar{v}^{r5}_{S5.5}/\omega$ and $\bar{v}^{r7}_{S5.7}/\omega$ for healthy motor (a)-(c), and for a rotor demagnetization of 10° (6.62%). (d)-(f). The motor is operating at 250 rpm and delivering the rated torque.

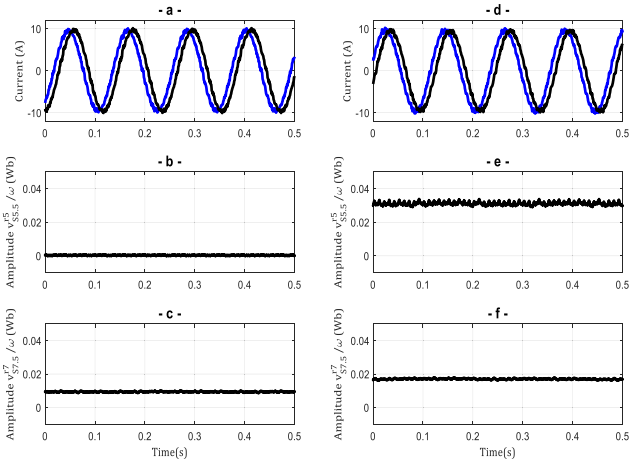

FIGURE 8. Experimental results: from top to bottom, waveforms of the stator currents in phase a1 and a2, magnitudes of the dc voltage space vectors $\bar{v}^{r5}_{S5.5}/\omega$ and $\bar{v}^{r7}_{S5.7}/\omega$ for healthy motor (a)-(c), and for a rotor demagnetization of 10° (6.62%). (d)-(f). The motor is operating at 250 rpm and delivering the rated torque.

However, observing the magnitude variation of the normalized dc voltage space vector $\bar{v}^{r5}_{S5.5}/\omega$, one can notice the significant increment in amplitude from healthy (Fig. 7-b) to 10° (6.62%) of RMD (Fig. 7-e).

The same observation is valid when comparing the contribution of the 7th harmonic from healthy (Fig. 7-c) to the same faulty condition (Fig. 7-f), but with a less relevant variation. The operating conditions of the simulation tests (Fig. 7) have been experimentally reproduced, leading to the results reported in Fig. 8. By comparing Fig. 7 and Fig. 8, it can be seen that the behavior of the normalized dc voltage space vectors $\bar{v}^{r5}_{S5.5}/\omega$ and $\bar{v}^{r7}_{S5.7}/\omega$, adopted for fault detection is not only confirmed by simulations, but also by experiments.

At this point of the investigation, the sensitivity of the normalized dc voltage space vectors, in terms of amplitude, is clearly evidenced. Thus, a high sensitivity of the proposed RMD fault index F_{dem}, that considers not only the magnitude variation of the normalized dc voltage space vectors $\bar{v}^{r5}_{S5.5}$ and $\bar{v}^{r7}_{S5.7}$, but also the phase variation caused by RMD, is expected.

Trend details of the RMD fault index F_{dem}, formulated by (14), and corresponding to the simulation results shown in Fig. 7, were computed under healthy and faulty conditions, and depicted in Fig. 9. Under healthy condition, the F_5 (Fig. 9-a) and F_7 (Fig. 9-b) indexes are equal to zero, leading to a zero value of the RMD fault index F_{dem} (Fig. 9-c). However, under a 10° (6.62%) of demagnetization, the same quantities F_5 (Fig. 9-a) and F_7 (Fig. 9-b) show significant variations, leading to a relevant quantitative fault signature cumulated by the proposed RMD fault index F_{dem} (Fig. 9-c). Details of the experimental trends of F_5, F_7, and F_{dem} indexes corresponding to Fig. 9, are reported in Fig. 10. Although the slight discrepancies that can be noted between the simulated and the experimental behavior of the F_5 and F_7 indexes, a good agreement is clearly evidenced for the proposed RMD fault index F_{dem}, when comparing Fig. 9-c and Fig. 10-c.

In Fig. 11, the behavior of the indexes F_5, F_7 and F_{dem}, computed by numerical simulations for different RMD degrees $\Delta\gamma$, and measured by experimental tests for healthy conditions and under a RMD of 10° (6.62%), is reported. It is evidenced that the F_5 (Fig. 11-a) and F_7 (Fig. 11-b) indexes increase with the increasing RMD fault severity, accordingly, leading to significant increments of the RMD fault index F_{dem} (Fig. 11-c). The good agreement between simulations and experiments confirms the sensitivity of the proposed RMD fault index F_{dem}.

It should be noted that under 10° (6.62%) of RMD, the discrepancies in simulations found for the F_5 (Fig. 11-a) and F_7 (Fig. 11-b) indexes, when compared to the experimental tests, can be ascribed to three main causes: modeling approximations of the magnet field distribution, the presence of unavoidable intrinsic rotor magnet asymmetries, and errors of the measurement devices.

V. ROBUSTNESS OF THE PROPOSED RMD FAULT INDEX

The results obtained in the previous section prove that the adopted RMD fault index F_{dem} is clearly sensitive to RMD affecting a six-phase PMSM. In the present section, the robustness of the proposed RMD fault index is evaluated under steady-state and time-varying conditions.

Being normalized by the angular speed ω, the F_5 and F_7 indexes, expressed in (15) and (16), respectively, are independent of speed, which in turns leads to a complete immunity of the adopted fault index F_{dem} against variable speed operating conditions. In Fig. 12-a, the RMD fault index calculated by simulations, is reported for different values of speed and load torque in steady-state conditions. The obtained results confirm the theoretical analysis, leading to a robust RMD fault index against speed variations.

Examining the dc voltage space vectors $\bar{v}^{r5}_{S5.5}$ and $\bar{v}^{r7}_{S5.7}$, expressed in (12) and (13) by $\bar{e}_{5.5}$ and $\bar{e}_{5.7}$, respectively, it is

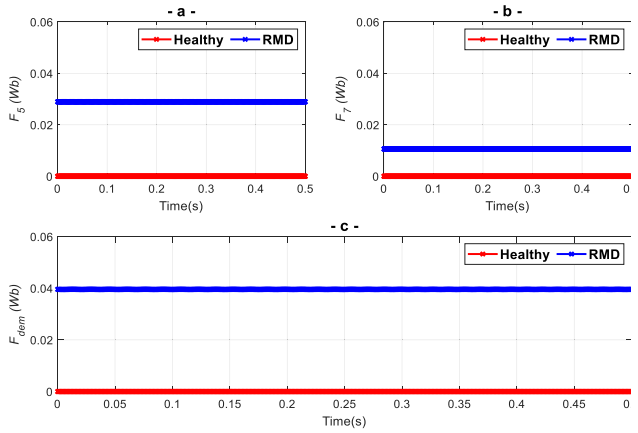

FIGURE 9. Simulation results: (a)-(b) instantaneous values of the F_5 and F_7 indexes, for healthy motor and under a RMD of 10° (6.62%). (c) instantaneous values of the proposed fault index F_{dem}, from healthy to 10° (6.62%) of RMD. The motor is operating at 250 rpm and delivering the rated torque.

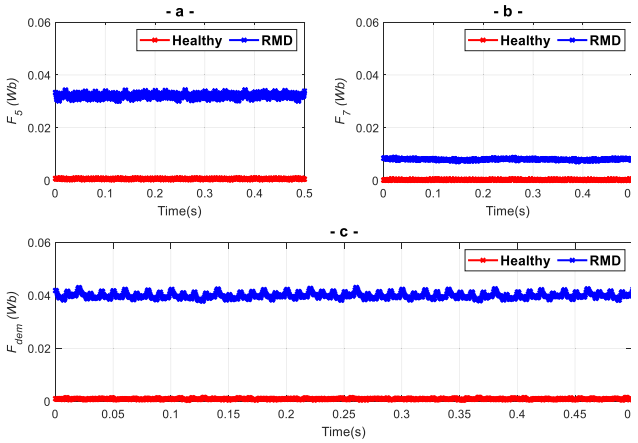

FIGURE 10. Experimental results: (a)-(b) instantaneous values of the F_5 and F_7 indexes, for healthy motor and under a RMD of 10° (6.62%). (c) instantaneous values of the proposed fault index F_{dem}, from healthy to 10° (6.62%) of RMD. The motor is operating at 250 rpm and delivering the rated torque.

evident that these two quantities, required for computing the fault index F_{dem}, are completely independent of load level. Aside the fact that the load conditions exclusively determine the current in plane d_1-q_1, the current regulators $PI_{+5,d}$, $PI_{+5,q}$, $PI_{-7,d}$ and $PI_{-7,q}$ are tuned to keep the current $i_{S5,ref}$ equal to zero. This conclusion has been confirmed by the simulation results reported in Fig. 12-b.

The corresponding experimental tests, under different speed and load levels, are reported in Fig. 13-a and Fig. 13-b, respectively, which are in agreement with the theoretical analysis and the simulation results reported in Fig. 12, confirming the robustness of RMD fault index against speed and load operating levels.

Eventually, some experimental tests were made with different values of the gains of the PI current regulators in the d_1-q_1 and d_5-q_5 planes. Fig. 14 shows the behavior of the proposed demagnetization fault index F_{dem} versus control parameters,

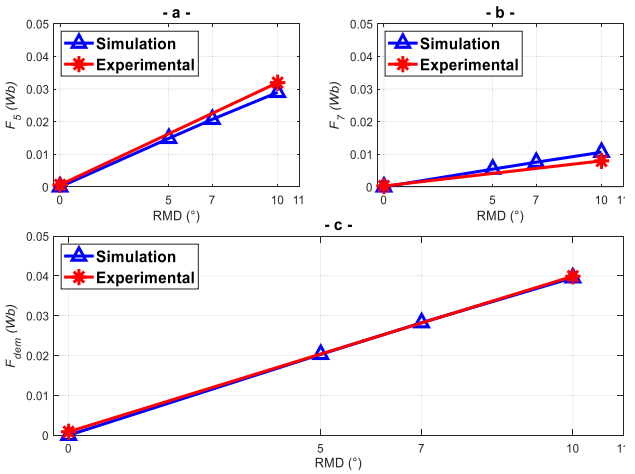

FIGURE 11. Simulation and experimental results: behavior of (a) F_5, (b) F_7, (c) F_{dem} indexes, versus low degrees of RMD: 0° (0%), 5° (3.31%), 7° (4.64%), 10° (6.62%). The motor is operating at 250 rpm and delivering the rated torque.

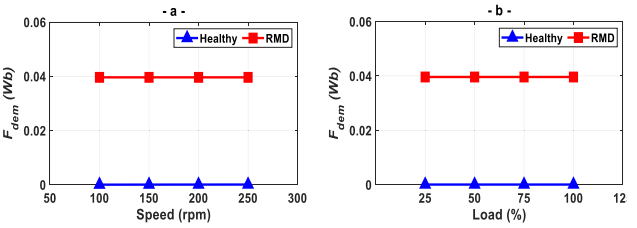

FIGURE 12. Simulation results: behavior of the proposed demagnetization fault index F_{dem}, from healthy to 10° (6.62%) of RMD under: a) different operating speeds and delivering rated torque, and b) constant speed of 250 rpm for different load operating conditions.

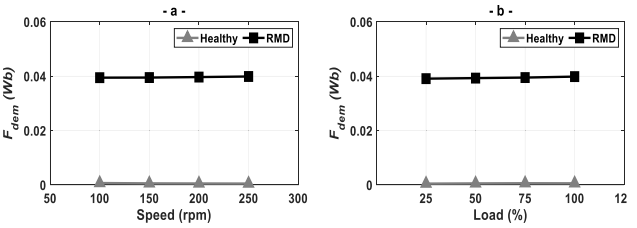

FIGURE 13. Experimental results: behavior of the proposed demagnetization fault index F_{dem}, from healthy to 10° (6.62%) of RMD under: a) different operating speeds and delivering rated torque, and b) constant speed of 250 rpm for different load operating conditions.

under 10° (6.62%) of RMD when the motor is operating at constant speed of 250 r/min and delivering the rated torque.

The results reported in Fig. 14-a, showing the influence of the parameter kp_1 on the fault index, have been obtained by setting $ki_1 = 0.2$ pu, $kp_5 = 0.9$ pu, $ki_5 = 0.5$ pu. The results reported in Fig. 14-b, showing the influence of the parameter ki_1 on the fault index, have been obtained by setting $kp_1 = 14$ pu, $kp_5 = 0.9$ pu, $ki_5 = 0.5$ pu. The results reported in Fig. 14-c, showing the influence of the parameter kp_5 on the fault index, have been obtained by setting $kp_1 = 9$ pu, $ki_1 = 0.5$ pu, $ki_5 = 0.5$ pu. Finally, the results reported in Fig. 14-d, showing the influence of the parameter ki_5 on the fault index,

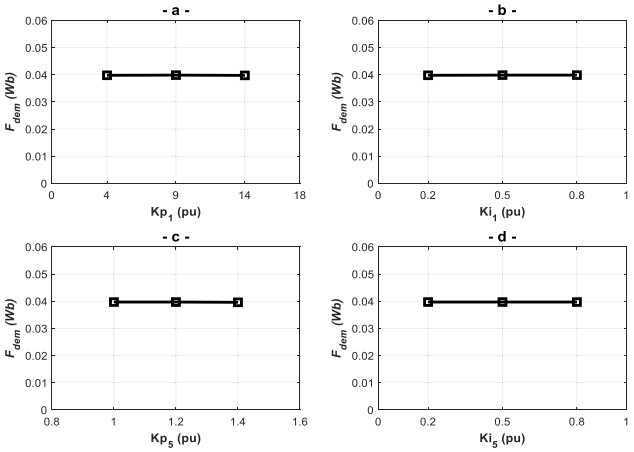

FIGURE 14. Experimental results: behavior of the proposed demagnetization fault index F_{dem} versus control parameters, under 10° (6.62%) of RMD. (a) Influence of the parameter kp1. (b) Influence of the parameter ki1. (c) Influence of the parameter kp5. (d) Influence of the parameter ki5. The motor is operating at 250 r/min and delivering the rated torque.

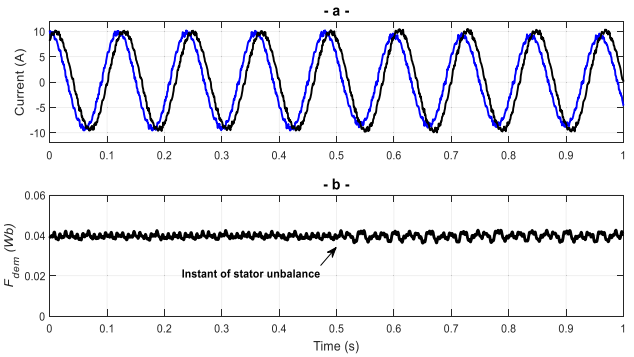

FIGURE 15. Experimental results: (a) waveforms of the stator currents in phase a1 and a2. (b) behavior of the proposed fault index F_{dem}, under 10° (6.62%) of RMD, and during a sudden stator unbalance. The motor is operating at 250 rpm and delivering the rated torque.

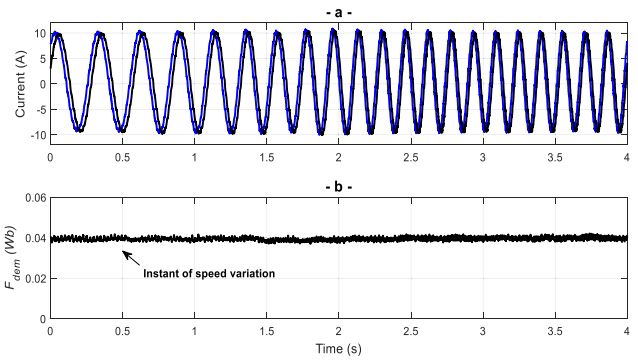

FIGURE 16. Experimental results: (a) waveforms of the stator currents in phase a1 and a2. (b) behavior of the proposed fault index F_{dem}, under 10° (6.62%) of RMD, and during a speed transient. The motor is delivering the rated torque.

have been obtained by setting $kp_1 = 9$ pu, $ki_1 = 0.5$ pu, $kp_5 = 0.9$ pu.

As can be evidenced, the proposed fault index F_{dem} is completely unsensitive to the parameters kp_1 and ki_1 in the first plane (Fig. 14-a and Fig. 14-b) nor to the parameters

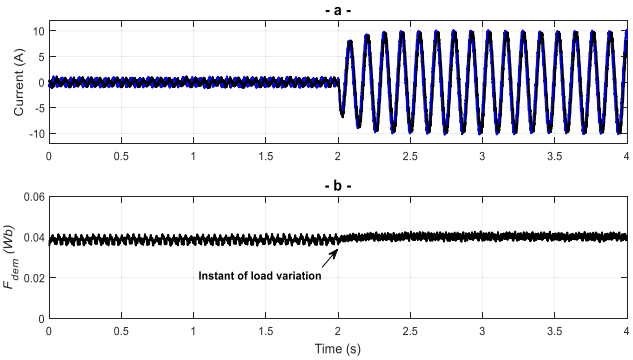

FIGURE 17. Experimental results: (a) waveforms of the stator currents in phase a1 and a2. (b) behavior of the proposed RMD fault index F_{dem}, under 10° (6.62%) of RMD, and during a load transient. The motor is delivering the rated torque.

kp_5 and ki_5 in the 5th plane (Fig. 14-c and Fig. 14-d). These experimental results corroborate the analytical predictions, where the formulated fault index in (14) and specifically computed by the quantities (12)-(13), is independent of the current regulators parameters.

To evaluate the robustness of the proposed RMD fault index under transient conditions, three important tests were performed using the six-phase PMSM affected by RMD.

The first test is aimed at the robustness evaluation of the RMD fault index F_{dem} during a sudden high-resistance connection affecting one phase and leading to a stator unbalance. The corresponding results are reported in Fig. 15. During the test, the motor was running at constant speed of 250 rpm and delivering the rated torque. At time t = 0.5 s, an increase of 50% of the phase resistance was applied to phase a1, leading to the unbalance that can be noted by examining the phase currents reported in Fig. 15-a. As can be evidenced in Fig. 15-b, before and after the introduced sudden stator unbalance, the RMD fault index level is practically unchanged, leading to a clear robustness against possible stator unbalanced conditions that can affect the machine.

The second test concerns a specific speed-varying conditions of the six-phase PMSM consisting in a speed ramp from 100 rpm to 200 rpm in a time interval of 1.5 s, when the motor is delivering the rated torque. When observing the obtained results in Fig. 16, the unsensitivity of the RMD fault index (Fig. 16-b) against a speed transient is evidenced. This result validates the interest in speed normalization applied in (15) and (16) to dc quantities.

The third test was performed under an abrupt load transient, when the motor is rotating at constant speed (250 rpm). The corresponding results are shown in Fig. 17. At time t = 2.0 s, a load variation from 0% to 100% was applied to the six-phase PMSM, leading to the current behavior reported in Fig. 17-a. As can be seen in Fig. 17-b, before and after the load variation, the fault index is practically constant, leading to a clear robustness versus load torque variations.

At this level of the investigations, it should be noted that previous RMD detection techniques based on the spectral analysis of the 5th and 7th harmonics of stator voltage space

vector in the α_5-β_5 plane [33], may fail during a speed transient, due to the spreading effect that affects the fault components of interest.

Conversely, it can be underlined that the proposed strategy allows an accurate quantitative statement of RMD that can affect a six-phase PMSM drive, even under time-varying operating conditions. In particular, the dc behavior of the fault index makes it possible to avoid any frequency variations during speed transient conditions, and the normalization with respect to ω allows the amplitude variations of the dc index to be offset. Beside to this, the fault index has shown a robustness also against possible stator unbalanced operating conditions. Taking the small effects of the temperature variation and the nearly linear dependence of the fault index on the RMD level into account (see Fig. 5), and considering the quality of the signal F_{dem} as extracted from the experimental tests (see Figs. 10c, 15, 16 and 17) the error on the estimated value of the RMD can be assumed close to $1 \div 2\%$.

VI. CONCLUSION

Multiphase PMSMs have a higher number of degrees of freedom when compared to standard three-phase PMSMs, which can be exploited not only to fault tolerance purposes, but also for effective fault diagnosis techniques. In this paper, a novel technique for diagnosing RMD affecting a vector-controlled asymmetrical six-phase surface-mounted PMSM has been proposed. The developed strategy is based on a fault index processed from the control signals synthetized in the 5^{th} plane, and already available in the control platform.

The analysis was limited to RMD involving a maximum of 14% of the pole arc as the aim of this paper is to detect incipient RMD. Higher values of RMD, even if detected, may lead to an irreversible deterioration of the motor performance. The analysis presented may show some limitations for high levels of RMD as the harmonics of the magnetic field distribution due to magnets become relevant and a more accurate modelling of the machine parameters would be necessary.

Based on the analytical developments tested by numerical simulations and experimental tests, it was shown that the proposed fault index is a sensitive indicator for detecting and quantifying RMD at incipient stage. It was also shown that the proposed fault index is highly robust against speed and load transients, and stator unbalance faults.

Finally, it is worth noting that the proposed strategy can be easily generalized for all the motor drive control techniques in which the value of the reference voltage space vector in subspace 5 is available.

REFERENCES

[1] E. Levi, "Multiphase electric machines for variable-speed applications," *IEEE Trans. Ind. Electron.*, vol. 55, no. 5, pp. 1893–1909, May 2008.

[2] F. Barrero and M. J. Duran, "Recent advances in the design, modeling, and control of multiphase machines—Part I," *IEEE Trans. Ind. Electron.*, vol. 63, no. 1, pp. 449–458, Jan. 2016.

[3] S. Ruoho, J. Kolehmainen, J. Ikaheimo, and A. Arkkio, "Interdependence of demagnetization, loading, and temperature rise in a permanent-magnet synchronous motor," *IEEE Trans. Magn.*, vol. 46, no. 3, pp. 949–953, Mar. 2010.

[4] J. Hong, D. Hyun, S. Bin Lee, J.-Y. Yoo, and K.-W. Lee, "Automated monitoring of magnet quality for permanent-magnet synchronous motors at standstill," *IEEE Trans. Ind. Appl.*, vol. 46, no. 4, pp. 1397–1405, Jul. 2010.

[5] E. Mazaheri-Tehrani and J. Faiz, "Airgap and stray magnetic flux monitoring techniques for fault diagnosis of electrical machines: An overview," *IET Electr. Power Appl.*, vol. 16, no. 3, pp. 277–299, Mar. 2022.

[6] V. I. Patel, J. Wang, and S. S. Nair, "Demagnetization assessment of fractional-slot and distributed wound 6-phase permanent magnet machines," *IEEE Trans. Magn.*, vol. 51, no. 6, pp. 1–11, Jun. 2015.

[7] S. S. Nair, V. I. Patel, and J. Wang, "Post-demagnetization performance assessment for interior permanent magnet AC machines," *IEEE Trans. Magn.*, vol. 52, no. 4, pp. 1–10, Apr. 2016.

[8] J. Faiz and E. Mazaheri-Tehrani, "Demagnetization modeling and fault diagnosing techniques in permanent magnet machines under stationary and nonstationary conditions: An overview," *IEEE Trans. Ind. Appl.*, vol. 53, no. 3, pp. 2772–2785, May 2017.

[9] S. Choi, M. S. Haque, M. T. B. Tarek, V. Mulpuri, Y. Duan, S. Das, V. Garg, D. M. Ionel, M. A. Masrur, B. Mirafzal, and H. A. Toliyat, "Fault diagnosis techniques for permanent magnet AC machine and drives—A review of current state of the art," *IEEE Trans. Transport. Electrific.*, vol. 4, no. 2, pp. 444–463, Jun. 2018.

[10] C. Mejuto, M. Mueller, M. Shanel, A. Mebarki, M. Reekie, and D. Staton, "Improved synchronous machine thermal modelling," in *Proc. 18th Int. Conf. Electr. Mach.*, Sep. 2008, pp. 1–6.

[11] A. J. Grobler, S. R. Holm, and G. van Schoor, "A two-dimensional analytic thermal model for a high-speed PMSM magnet," *IEEE Trans. Ind. Electron.*, vol. 62, no. 11, pp. 6756–6764, Nov. 2015.

[12] D. Liang, Z. Q. Zhu, J. H. Feng, S. Y. Guo, Y. F. Li, A. F. Zhao, and J. W. Hou, "Estimation of 3-D magnet temperature distribution based on lumped-parameter and analytical hybrid thermal model for SPMSM," *IEEE Trans. Energy Convers.*, vol. 37, no. 1, pp. 515–525, Mar. 2022.

[13] J.-C. Urresty, R. Atashkhooei, J.-R. Riba, L. Romeral, and S. Royo, "Shaft trajectory analysis in a partially demagnetized permanent-magnet synchronous motor," *IEEE Trans. Ind. Electron.*, vol. 60, no. 8, pp. 3454–3461, Aug. 2013.

[14] Z. Yang, X. Shi, and M. Krishnamurthy, "Vibration monitoring of PM synchronous machine with partial demagnetization and inter-turn short circuit faults," in *Proc. IEEE Transp. Electrific. Conf. Expo (ITEC)*, Jun. 2014, pp. 1–6.

[15] G. A. Skarmoutsos, K. N. Gyftakis, and M. Mueller, "Detecting partial demagnetization in AFPM generators by monitoring speed and EMF induced in a supplemental winding," *IEEE Trans. Ind. Informat.*, vol. 18, no. 5, pp. 3295–3305, May 2022.

[16] C. Wang, M. D. Prieto, L. Romeral, Z. Chen, F. Blaabjerg, and X. Liu, "Detection of partial demagnetization fault in PMSMs operating under nonstationary conditions," *IEEE Trans. Magn.*, vol. 52, no. 7, pp. 1–4, Jul. 2016.

[17] A. G. Espinosa, J. A. Rosero, J. Cusido, L. Romeral, and J. A. Ortega, "Fault detection by means of Hilbert–Huang transform of the stator current in a PMSM with demagnetization," *IEEE Trans. Energy Convers.*, vol. 25, no. 2, pp. 312–318, Feb. 2010.

[18] J.-C. Urresty, J.-R. Riba, M. Delgado, and L. Romeral, "Detection of demagnetization faults in surface-mounted permanent magnet synchronous motors by means of the zero-sequence voltage component," *IEEE Trans. Energy Convers.*, vol. 27, no. 1, pp. 42–51, Mar. 2012.

[19] J.-C. Urresty, J.-R. Riba, and L. Romeral, "A back-EMF based method to detect magnet failures in PMSMs," *IEEE Trans. Magn.*, vol. 49, no. 1, pp. 591–598, Jan. 2013.

[20] T. Goktas, M. Zafarani, K. W. Lee, B. Akin, and T. Sculley, "Comprehensive analysis of magnet defect fault monitoring through leakage flux," *IEEE Trans. Magn.*, vol. 53, no. 4, pp. 1–10, Apr. 2017.

[21] D. Reigosa, D. Fernández, Y. Park, A. B. Diez, S. B. Lee, and F. Briz, "Detection of demagnetization in permanent magnet synchronous machines using Hall-effect sensors," *IEEE Trans. Ind. Appl.*, vol. 54, no. 4, pp. 3338–3349, Jul. 2018.

[22] Y. Park, C. Yang, S. B. Lee, D. Lee, D. Fernandez, D. Reigosa, and F. Briz, "Online detection and classification of rotor and load defects in PMSMs based on Hall sensor measurements," *IEEE Trans. Ind. Appl.*, vol. 55, no. 4, pp. 3803–3812, Jul. 2019.

[23] H. Chen, C. X. Gao, J. Si, Y. Nie, and Y. Hu, "A novel method for diagnosing demagnetization-fault in PMSM using toroidal-yoke-type search coil," *IEEE Trans. Instrum. Meas.*, vol. 71, pp. 1–12, 2022.

[24] K. N. Gyftakis, S. A. Rasid, G. A. Skarmoutsos, and M. Mueller, "The demagnetization harmonics generation mechanism in permanent magnet machines with concentrated windings," *IEEE Trans. Energy Convers.*, vol. 36, no. 4, pp. 2934–2944, Dec. 2021.
[25] J.-R.-R. Ruiz, J. A. Rosero, A. G. Espinosa, and L. Romeral, "Detection of demagnetization faults in permanent-magnet synchronous motors under nonstationary conditions," *IEEE Trans. Magn.*, vol. 45, no. 7, pp. 2961–2969, Jul. 2009.
[26] A. G. Yepes, O. Lopez, I. Gonzalez-Prieto, M. J. Duran, and J. Doval-Gandoy, "A comprehensive survey on fault tolerance in multiphase AC drives, Part 1: General overview considering multiple fault types," *Machines*, vol. 10, no. 3, p. 208, Mar. 2022.
[27] A. Khoobroo and B. Fahimi, "A novel method for permanent magnet demagnetization fault detection and treatment in permanent magnet synchronous machines," in *Proc. 25th Annu. IEEE Appl. Power Electron. Conf. Expo. (APEC)*, Feb. 2010, pp. 2231–2237.
[28] Y. Zafari, A. H. Mazinan, and S. Shoja-Majidabad, "Demagnetization fault detection for five-phase IPMSM through integral terminal sliding mode flux-linkage observer," *IETE J. Res.*, vol. 65, no. 4, pp. 473–486, Jul. 2019.
[29] Y. Gritli, A. Tani, C. Rossi, and D. Casadei, "Assessment of current and voltage signature analysis for the diagnosis of rotor magnet demagnetization in five-phase AC permanent magnet generator drives," *Math. Comput. Simul.*, vol. 158, pp. 91–106, Apr. 2019.
[30] C. Candelo-Zuluaga, J.-R. Riba, D. V. Thangamuthu, and A. Garcia, "Detection of partial demagnetization faults in five-phase permanent magnet assisted synchronous reluctance machines," *Energies*, vol. 13, no. 13, p. 3496, Jul. 2020.
[31] Y. Gritli, A. Tani, C. Rossi, and D. Casadei, "Detection of rotor magnet demagnetization in asymmetrical six-phase surface mounted permanent magnet synchronous motor drive," in *Proc. 13th Int. Conf. Electr. Mach. (ICEM)*, Sep. 2018, pp. 1809–1814.
[32] K. Zhao, A. Leng, R. Zhou, W. Dai, S. Wu, and T. Li, "Demagnetization fault reconstruction for six-phase permanent magnet synchronous motor by improved super-twisting algorithm-based sliding-mode observer," *Measurement*, vol. 172, Jan. 2021, Art. no. 108905.
[33] Y. Gritli, M. Mengoni, G. Rizzoli, C. Rossi, A. Tani, and D. Casadei, "Rotor magnet demagnetisation diagnosis in asymmetrical six-phase surface-mounted AC PMSM drives," *IET Electr. Power Appl.*, vol. 14, no. 10, pp. 1747–1755, Oct. 2020.
[34] Y. Gritli, D. Casadei, A. Tani, C. Rossi, and G. Serra, "Validation of rotor magnets demagnetization detection in six-phase surface-mounted AC permanent magnet synchronous motors," in *Proc. Int. Symp. Power Electron., Electr. Drives, Autom. Motion (SPEEDAM)*, Jun. 2018, pp. 224–229.
[35] Y. Gritli, M. Mengoni, C. Rossi, A. Tani, D. Casadei, and G. Serra, "Experimental assessment of winding inter-turn short-circuits fault signatures in six-phase AC permanent magnet synchronous motors," *IET Renew. Power Gener.*, vol. 14, no. 15, pp. 2791–2800, 2020.

YASSER GRITLI (Member, IEEE) received the M.Sc. degree in electrical engineering from the University of Tunis El Manar, Tunisia, in 2006, and the Ph.D. degree in electrical engineering from the University of Bologna, Italy, in 2014. In 2012, he joined the LARA-ENIT Research Group, University of Tunis El Manar, as a Researcher. He is currently a Research Fellow with the University of Bologna. His research interests include electric drive design and diagnosis of multiphase machines for automotive and renewable energy applications.

CLAUDIO ROSSI (Member, IEEE) received the M.Sc. degree, in 1997, and the Ph.D. degree, in 2001. He was a Faculty Advisor of the Ondasolare Team, where he built the solar car "Emilia 4." Since 2015, he has been an Associate Professor of electrical machines, drives and power electronics with the University of Bologna. He is the author of 145 articles and ten patents. His research interests include ac drives and energy storage systems for electric traction applications. He is the winner of the American Solar Challenge, in 2018.

GABRIELE RIZZOLI received the M.Sc. and Ph.D. degrees in electrical engineering from the University of Bologna, Bologna, Italy, in 2012 and 2016, respectively. He is currently a Junior Assistant Professor with the Department of Electrical, Electronic and Information Engineering "Guglielmo Marconi," University of Bologna. His research interests include the design of electrical machines, the development and control of high-efficient power converters for automotive, and renewable energy applications.

MICHELE MENGONI (Member, IEEE) received the M.S. (Hons.) and Ph.D. degrees in electrical engineering from the University of Bologna, Bologna, Italy, in 2006 and 2010, respectively. He is currently an Associate Professor with the Department of Electric, Electronic and Information Engineering "Guglielmo Marconi," University of Bologna. His research interests include design, analysis, and the control of three phase electric machines, multiphase drives, and ac/ac matrix converters.

ANGELO TANI received the M.Sc. degree (Hons.) in electrical engineering from the University of Bologna, Bologna, Italy, in 1988. Currently, he is a Full Professor of power electronics, electrical machines and drives with the Department of Electrical, Electronic and Information Engineering "Guglielmo Marconi," University of Bologna. He has authored more than 200 papers published in technical journals and conference proceedings. His current research interests include modeling, control, and the fault diagnosis of multiphase electric machines.

DOMENICO CASADEI received the M.Sc. degree (Hons.) in electrical engineering from the University of Bologna, Italy, in 1974. He is currently a Full Professor of electrical drives with the Department of Electrical, Electronic, and Information Engineering "Guglielmo Marconi," University of Bologna. He is the author and the coauthor of more than 300 scientific papers published in technical journals and conference proceedings. His research interests include the vector control of ac drives and the diagnosis of electrical machines. He is a member of the IEEE Industrial Electronics Society, the IEEE Power Electronics Society, and the European Power Electronics Society. He has been elevated to the grade of IEEE Fellow for contributions to direct torque control and matrix converters in electric drives.

Open Access funding provided by 'Alma Mater Studiorum - Università di Bologna' within the CRUI CARE Agreement